



Catalytic oxidation of toluene by $\text{SrTi}_{1-x}\text{B}_x\text{O}_3$ (B = Cu and Mn) with dendritic morphology synthesized by one pot hydrothermal route



S.I. Suárez-Vázquez ^{a,b,*}, S. Gil ^b, J.M. García-Vargas ^b, A. Cruz-López ^a, A. Giroir-Fendler ^{b,*}

^a Universidad Autónoma de Nuevo León, Facultad de Ingeniería Civil, Av. Universidad S/N, Ciudad Universitaria, San Nicolás de los Garza, Nuevo León, 66455, México

^b Univ. Lyon, Université Claude Bernard Lyon 1, CNRS, IRCELYON, 2 avenue Albert Einstein, Villeurbanne, F-69622, France

ARTICLE INFO

Article history:

Received 27 September 2016

Received in revised form 13 February 2017

Accepted 12 April 2017

Available online 15 April 2017

Keywords:

Volatile organic compounds

Toluene

Catalytic oxidation

Perovskite

ABSTRACT

This work is focus in the effect of B-site cations of SrTiO_3 perovskites with non-common morphology (dendritic) on the catalytic behavior of the toluene oxidation reaction. SrTiO_3 perovskites doped by two different transition metals (Cu or Mn) were synthesized by the one pot hydrothermal method and characterized by several techniques. The perovskite structure and the dendritic morphology were confirmed by XRD and SEM analyses for all catalysts. In addition, similar textural properties were observed among the catalysts. The addition of metal-dopants provides good stability during three catalytic cycles and in the lifetime test. However, segregation of Cu as CuO was observed on the surface of the Cu-doped catalyst. In contrast, the addition of Mn resulted in the incorporation of Mn^{4+} in Ti^{4+} sites present into the structure of the perovskite. This incorporation also enhances the relation $\text{O}_{\text{ads}}/\text{O}_{\text{latt}}$ and the catalytic properties. Finally, the catalyst doped by Mn presented the highest catalytic activity with complete conversion of toluene to CO_2 at temperatures below 350 °C.

© 2017 Elsevier B.V. All rights reserved.

1. Introduction

Volatile organic compounds (VOCs) are becoming one of the biggest gaseous pollutants, attracting wide attention not only because of their air pollutant effects like photochemical smog and greenhouse effect, but also due to their toxic, mutagenic and carcinogenic properties reported on the human health [1,2]. Therefore, some organizations around the world have been introducing stringent regulations to control their emissions [3–5]. Among the VOCs, toluene has been considered as one of the 189 hazardous air pollutants listed in the 1990 Clean Air Act Amendment (CAA90) proposed by the US Environmental Agency [5].

Several strategies for the elimination of toluene have been proposed recently such as biodegradation [6,7], adsorption [8,9], photocatalysis [10–12] and oxidative catalysis [13–17]. Among the catalytic alternatives, perovskite-type oxides with ABO_3 structure have been widely used and considered the most promising catalysts

for VOCs pollutants removal, due to their low operation temperature, their adequate catalytic activity, high oxygen mobility, redox properties, good thermal stability, adaptability and low cost compared with the precious and transition metal oxides. Moreover, these features can be controlled by partial or total substitution of A- and/or B-site cations with different metals, altering the oxidation state or the redox properties of cations and the surface oxygen vacancies, which have a direct influence on the catalytic performance [18–21]. Thus, these undoped and doped perovskite-type oxides have been extensively studied in last years. Zhang et al. reported the complete catalytic oxidation of toluene below 350 °C without any deactivation of the catalyst using LaMnO_3 prepared by three different methods [16]. Ji et al. showed the degradation of 90% of toluene around 305 °C using the perovskite $\text{Eu}_{1-x}\text{Sr}_x\text{FeO}_3$ [17]. Li et al. reported the decomposition of toluene at temperatures below 300 °C introducing Sr and Fe into the perovskite LaCoO_3 . They attributed the high catalytic activity observed for these catalysts to the increase in the amount of weakly adsorbed oxygen produced by the higher quantity of oxygen vacancies that the introduction of these two metals (Sr and Fe) induce in the perovskites [22]. In addition, the H_2 -production by steam reforming of toluene have also been evaluated using the perovskite LaAlO_3 as support in a Ni/LaAlO_3 catalyst where the 30% of the La sites were replaced by Sr [23]. From these reports we can observe that different type of perovskite have been tested for catalytic abatement of toluene, using

* Corresponding authors at: +(52) +(81)8329400 Ext. 7256 (S.I. Suárez-Vázquez) Universidad Autónoma de Nuevo León and +(33) 4 72431586 (A. Giroir-Fendler) Université Claude Bernard Lyon 1.

E-mail addresses: ssuarezvazquez@gmail.com, santiago.suarezvz@uanl.edu.mx (S.I. Suárez-Vázquez), anne.giroir-fendler@ircelyon.univ-lyon1.fr (A. Giroir-Fendler).

cations as La, Eu, Sr, etc. in A-site and Mn, Co, Fe, etc. in B-site, being the redox properties of the later an important factor to take into account.

Among the different reported perovskites, strontium titanate perovskite (SrTiO_3) doped with different cations has been widely studied as photocatalyst, catalyst and catalytic support for pollution removal and/or environmental protection due to its easily adjustable properties that can be modified by changing the oxygen stoichiometry after doping with foreign elements [24–35]. In particular, the Cu-doped SrTiO_3 perovskite prepared by sol-gel method has been reported as an excellent catalyst for the soot combustion and NO_x reduction [26,27]. Białobok et al. [34] and Ura et al. [29] reported the effect over the physico-chemical and catalytic properties in soot combustion of alkalies (Li, K, Cs) incorporation in the A-site of a SrTiO_3 perovskite, showing that the altered redox properties after doping have an important role on their catalytic activity and stability. Moreover, Yoon et al. reported that the partial substitution of titanium by a transition metal cation promoted the formation of oxygen vacancies and reduced the oxidation state of titanium on the SrTiO_3 perovskite, modifying the methane oxidation activity [35]. Recently, Wu et al. reported the photocatalytic degradation of tetracycline under visible light using SrTiO_3 doped with Mn in concentration around 3–7 at.% [28]. Therefore, although catalytic properties of raw SrTiO_3 perovskites are still limited, one could expect that due to their high thermal stability, adaptability and modifiable oxidative properties they can be applied as promising active catalyst for toluene combustion.

Moreover, it is well known that the synthesis methods greatly influence the physico-chemical and catalytic properties of perovskites [16,36,37]. For this reason, SrTiO_3 perovskites have been synthesized by different routes during the last years [29–31,35,38–41]. Among them, the hydrothermal synthesis can be carried out at relative low temperatures and very rapid crystallization rates, allowing to control the morphology and size of this perovskite [38]. Recently, Nishiro et al. prepared SrTiO_3 co-doped with rhodium and antimony by hydrothermal route using TiO_2 and $\text{Sr(OH)}_2 \cdot 8\text{H}_2\text{O}$ as precursors. They reported that rhodium species doped in SrTiO_3 affects the evolution of H_2 and O_2 during water splitting [30]. Huang et al. also reported the hydrothermal synthesis of SrTiO_3 but this time using P25- TiO_2 and $\text{Sr(OH)}_2 \cdot 8\text{H}_2\text{O}$ as starting materials and temperatures from 100 to 180 °C during 24–96 h. They mentioned the promotion of spherical shape of the perovskite by adding NaOH at different concentrations [31]. Zhen et al. achieved the hydrothermal synthesis of SrTiO_3 at 180 °C for 6 h using TiO_2 as Ti precursor. This material showed good photocatalytic activity in the photoreduction of Cr (VI) [39]. Jayabal et al. also reported the hydrothermal synthesis of SrTiO_3 applying an additional thermal treatment at 900 °C for 6 h to eliminate organic impurities [40]. Mourao et al. reported the rapid hydrothermal synthesis of this perovskite with assistance of mechanical stirring during the hydrothermal process [41].

Taking into account the lot of applications of SrTiO_3 in the environmental field and the wide range of advantages that the hydrothermal route offers, in this work the SrTiO_3 perovskite and Mn- and Cu-doped SrTiO_3 perovskites were prepared by a one pot hydrothermal route, characterized by various techniques and tested on the toluene catalytic oxidation with the aim to evaluate the effect of Mn- and Cu-doping on physico-chemical and redox properties of the B-site ($\text{Ti}^{\text{IV}}/\text{Ti}^{\text{III}}$) in $\text{SrTi}_{1-x}\text{B}_x\text{O}_3$, as well as on the catalytic performance. To our best knowledge, this is the first report dealing with catalytic performance of synthesized Cu or Mn substitute perovskites oxides SrTiO_3 with dendritic morphology in catalytic oxidation of toluene, while there are only a few reports regarding the one pot hydrothermal synthesis of SrTiO_3 doped with Cu and Mn.

2. Experimental

2.1. Catalysts preparation

Doped and undoped catalysts of SrTiO_3 were prepared by one pot hydrothermal method. Titanium butoxide (>97%, Sigma Aldrich Co.) and $\text{Sr}(\text{NO}_3)_2$ (>99%, Sigma Aldrich Co.) were used as precursors, which were mixed in stoichiometric ratios with 60 mL of NaOH 0.2 M to obtain an homogeneous solution. For doped-catalysts, calculated amount of $\text{Cu}(\text{NO}_3)_2 \cdot 3\text{H}_2\text{O}$ (>99%, Prolabo Fr.) and $\text{Mn}(\text{NO}_3)_2 \cdot 4\text{H}_2\text{O}$ (>97%, Sigma Aldrich Co.) to obtain 4%wt. of the metal-doped with chemical formula as $\text{SrTi}_{0.89}\text{Cu}_{0.11}\text{O}_3$ and $\text{SrTi}_{0.86}\text{Mn}_{0.14}\text{O}_3$ were added. After mixing, the final solution was placed into a Teflon vessel with 100 mL of volume and was hydrothermally treated at 180 °C for 24 h. When the thermal treatment was finished the solution was cooled to room temperature. Then, the powder was separate from the solution by decantation and washed gently with distilled water until neutral pH. Finally, the powder was dried at 105 °C for 6 h in room atmosphere and calcinated at 600 °C during 5 h under air flow of 50 mL/min with heating and cooling rates of 5 °C/min.

2.2. Catalysts characterization

The phase composition of the perovskites were evaluated by X-Ray Diffraction (XRD) in a Bruker D5005 diffractometer with $\text{CuK}\alpha$ radiation ($\lambda = 1.5418 \text{ \AA}$) and a scanning and step size of 0.5 s and 0.02° respectively. The mean crystallite size (d_s) of the perovskites was calculated using the Scherrer equation (Eq. (1)) [42]:

$$d_s = \frac{k \times \lambda}{\beta \times \cos(\theta)} \quad (1)$$

where d_s is the mean crystallite size, k is the shape factor (0.9), λ is the x-ray wavelength (1.54 Å), β is the broadening at half of the maximum intensity (FWHM), and θ is the Bragg angle. The morphology, particle size and elemental composition were observed by scanning electron microscopy (SEM-EDS) JEOL 6490 LV.

N_2 adsorption-desorption isotherms was carried out at –196 °C on a Micrometrics Tristar 3000 equipment. Before the measurement all catalysts were degassed at 350 °C for 3 h. The specific surface area of each catalyst was obtained by the Brunauer-Emmett-Teller (BET) method.

X-ray photoelectron spectroscopy analyses (XPS) were recorded on a Thermo ESCALAB 250 electron spectrometer with a monochromatized Al $\text{K}\alpha$ X-Ray source (1486.6 eV) and passing energy of 40 eV. C1 s (binding energy 284.8 eV) of formed carbon was used as a reference. XPS spectra were deconvoluted using XPSPEAK 41 program by the curve fitting after the Shirley-type background subtraction.

Finally, temperature-programmed reduction (TPR) experiments were conducted in a commercial BELcat unit with TCD detection. Catalyst (ca. 0.1 g) were loaded into a U-shaped tube and ramped from room temperature to 1173 K (10 K/min), using a reducing gas mixture of 5% v/v H_2/Ar (50 cm³/min).

2.3. Toluene catalytic test

The catalytic tests were carried out using 100 mg of catalyst and 400 mg of SiC to avoid hot spots, placed in a quartz cell in a U-type reactor. Synthetic air (80/20) was introduced to the reactor and the temperature was increased up to 80 °C using a heating rate of 5 °C/min and then kept at this value for 30 min. When this temperature was reached a mixture containing 1000 ppm of toluene and synthetic air (80/20) at 100 mL/min was introduced to the reactor. Once the 30 min at 80 °C were finished, the temperature

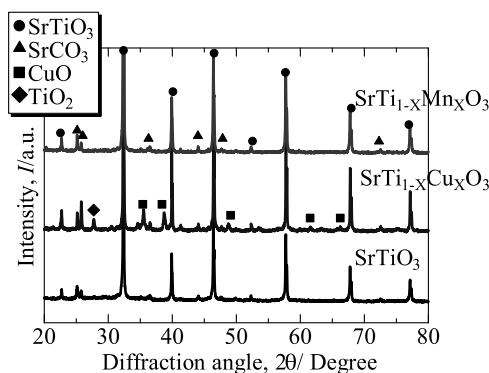


Fig. 1. X-Ray Diffractograms of perovskites synthesized in this work by hydrothermal method and calcined at 600 °C.

was increased to 450 °C using a heating rate of 2 °C/min and after that kept at this temperature during 60 min. After this treatment, all catalysts were also tested during the cooling ramp. Each catalytic test was repeated three times and reproducible results were successfully obtained.

Furthermore, the catalytic stability was also evaluated with long term experiments of 36 h at 50% of toluene conversion for all catalysts. The CO and CO₂ produced by the total conversion of toluene were measured in-situ by IR analyzer using a Rosemount Xtreme Gas Analyzer (Emerson Electric Co.). The conversion of toluene was defined as a function of the amount of CO₂ produced as it is shown in Eq. (2):

$$C_7H_8 (\%) = \frac{[CO_2]_i - [CO_2]_0}{7000 \text{ ppm}} \times 100 \quad (2)$$

where [CO₂]_i and [CO₂]₀ represents the CO₂ concentration measured every minute during the reaction and CO₂ concentration in the beginning of the reaction respectively.

3. Results and discussion

3.1. Physicochemical characterization of perovskites

Fig. 1 shows the diffractograms obtained in the XRD experiments for both the doped and undoped perovskites after calcination. For all the catalysts, diffraction peaks corresponding to that of the perovskite SrTiO₃ can be clearly identified, according with the card PDF-04-007-0044. However, some impurities as SrCO₃ were also identified in all catalysts. The formation of SrCO₃ is already reported during the SrTiO₃ synthesis by sol-gel and hydrothermal. This formation was attributed to the high Sr²⁺ solubility and its reaction with the CO₂ from the atmosphere which is dissolved into the water and the higher stability of carbonates at lower pH than the perovskites precipitating as SrCO₃ [26,31,43]. Other possibility for the formation of SrCO₃ falls on the Ti precursor because titanium butoxide can produce alkoxy radicals after its hydrolysis and it can be mineralized to CO₂, which contribute for the carbonate formation. On the other hand, the perovskite doped with Cu also shows some traces of CuO and TiO₂ indicating the possible segregation of CuO [26]. In contrast, the catalyst doped with Mn showed no evidence by XRD of the formation of any type of manganese oxide, besides the perovskite formation. This behavior can be explained in terms of ionic radius. It is well known that Mn⁴⁺ (0.53 Å) have lower ionic radius than Ti⁴⁺ (0.61 Å) with the same coordination number of 6, allowing the incorporation of Mn⁴⁺ in Ti⁴⁺ sites. However, Cu²⁺ (0.73 Å) has higher ionic radius than Ti⁴⁺, hampering the incorporation of the first in Ti⁴⁺ sites, resulting in the segregation of CuO on the surface as observed by XRD. The crystallite size of each catalyst is shown in **Table 1**. All sizes

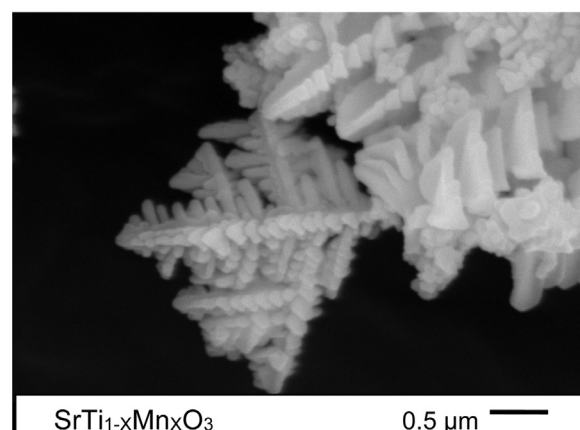
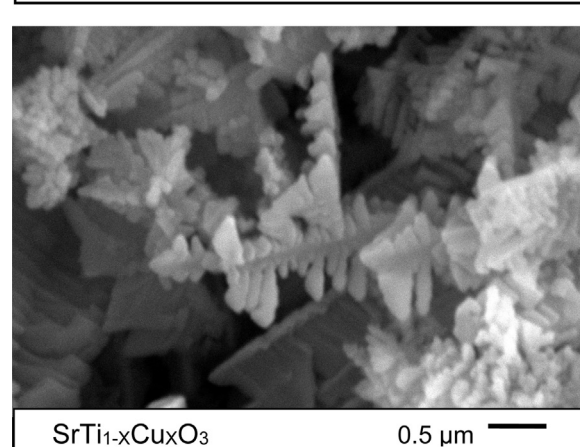
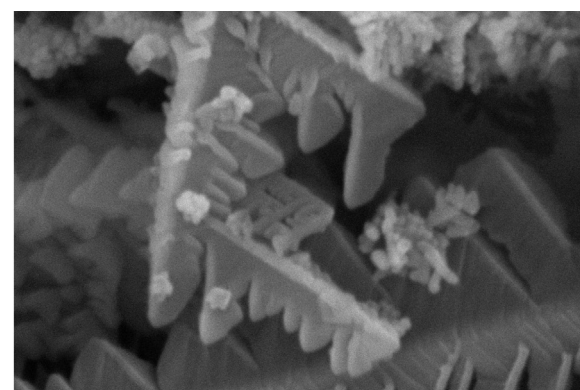


Fig. 2. SEM images of perovskites with dendritic morphology synthesized in this work by hydrothermal method and calcined at 600 °C.

are in the same order of magnitude and no substantial difference is observed among them. However, catalyst doped by Cu have slightly the highest crystallite size.

SEM images are shown in **Fig. 2**. Dendritic morphology with some branches is observed in all catalysts, which can contribute to enhance the surface area of these perovskites. The size of the branches in the dendrites is below 0.5 μm. No clear differences in size or shape was detected among catalysts, indicating that the addition of metal dopants does not have influence in the morphology. The formation of dendrites is attributed to the precursor of Ti and a diffusion-limited process in the hydrothermal reaction. In our reaction, titanium hydroxide (Ti(OH)₄) is formed during the mixing of the reagents with water at high pH values. According with thermodynamic calculation reported previously, the relative

Table 1

Textural, superficial and redox properties of perovskites synthesized in this work by the hydrothermal method and calcined at 600 °C.

Sample	Crystallite size d_s (nm)	Surface area (m ² /g)	Pore Volume (cm ³ /g)	Mean pore size (nm)	[O _{ads}]/[O _{lat}]	H ₂ consumption (mmol/g)	Reduction degree (%)
						Low Temp. peak	High Temp. peak
SrTiO ₃	60	28	0.14	10	0.05	–	0.229
SrTi _{1-x} Cu _x O ₃	84	26	0.14	11	0.06	0.549	0.230
SrTi _{1-x} Mn _x O ₃	70	22	0.14	13	0.11	0.173	0.283
							77.8
							48.7

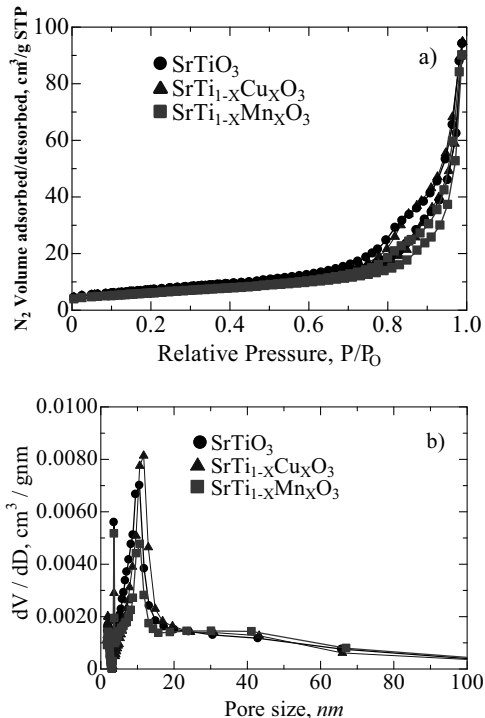


Fig. 3. Textural analysis of perovskites synthesized in this work: a) N₂ adsorption-desorption isotherms and b) Pore size distribution.

supersaturation increases as function of the temperature and the precursor solubility, having the Ti(OH)₄ high solubility values [38]. This supersaturation under hydrothermal conditions promotes an increase in the density of the reaction media and the formation of a restricted Ti soluble species resulting in a diffusion-limited process. Moreover, thermodynamics calculation reported previously [38] showed the high availability of Sr²⁺ species in these type of reactions. The instability of the front growth and the tendency of the perovskite phase to grow faster in the edge region of these restricted Ti soluble species promotes the nucleation of the perovskite into an irregular branching pattern as was previously reported by Kalyani et al. [38]. Oaki et al. also reported the promotion of the formation of skeletal, dendritic and branched forms in different inorganic crystals attributed to diffusion-limited rates of solutes or supersaturation controlled with different solvents [44].

Fig. 3 shows the N₂ adsorption-desorption isotherms and pore size distribution of catalysts prepared. All catalysts showed a hysteresis cycle, which is characteristic of the isotherm type IV (Fig. 3a). The hysteresis in this type of isotherm indicates the existence of capillary condensation, which is representative of a mesoporous material [45]. Fig. 3b shows the pore size distribution for all catalysts where clearly defined peaks around 10 nm are observed and confirms the existence of mesoporous as is mentioned above. In addition, Table 1 shows the surface area, pore volume and average pore size for each catalyst. Similar results are observed among the undoped and Cu-doped catalysts, whereas the catalyst doped

Table 2
Quantitative characterization of the perovskites surface measured by XPS (at%).

Sample	O	Ti	C	Sr	Cu	Mn
SrTiO ₃	51.98	16.49	13.86	17.67	–	–
SrTi _{1-x} Cu _x O ₃	51.24	15.67	15.20	15.78	2.10	–
SrTi _{1-x} Mn _x O ₃	52.31	14.26	14.56	15.03	–	3.84

by Mn reveals small superficial changes probably due to the complete insertion of Mn into the structure. It is worthy to mention the higher surface area and pore volume of perovskites materials obtained in this work, related with their morphology with dendritic shapes and/or the synthesis method selected; compared with previous reports where usually present lower surface area [26,31]. This is one of most important limitation of these materials for broader application in catalysis, resulting from high calcination temperature necessary to promote their crystallization.

Fig. 4a shows the general spectra obtain by the XPS experiments for those catalysts prepared. It can be clearly observed some peaks located at 132.5 eV, 457.9 eV and 529.1 eV which correspond to the Sr 3d, Ti 2p and O 1s respectively in SrTiO₃ [28,46]. In addition, the peaks of Cu 2p and Mn 2p at 932 eV and 641.5 eV are also observed in those Cu- and Mn-doped catalysts, respectively. On the other hand, Fig. 4b shows the characteristic peak of Cu, which can be deconvoluted in two main peaks at 932.6 and 934.0 eV. López-Suárez et al. [26] attributed the peak of Cu at 932.5 eV to the incorporation of Cu within the structure of SrTiCuO₃. The peak observed at 934.0 eV can be attributed to the specie Cu²⁺, being its predominance consistent with the peak of CuO observed in the XRD results (Fig. 1) [26]. In Fig. 4c two peaks exist at 641.5 and 653.2 eV which are described as Mn 2p^{3/2} and Mn2p^{1/2}, respectively. Because of the similar binding energy values for the Mn 2p^{3/2} among Mn²⁺ (640.9 eV), Mn³⁺ (641.2 eV) and Mn⁴⁺ (641.9 eV) is difficult to accurately quantify the Mn oxidation degree from this spectra. However, Hernández et al. [46] concluded, in assistance with the H₂-TPR, that the Mn specie that yields a peak at 641.6 eV corresponds to a Mn with an oxidation degree between 3+ and 4+. In addition, taking into account the similarity of the ionic radius between Ti⁴⁺ (0.68 Å) and Mn⁴⁺ (0.67 Å) we can deduce that Mn⁴⁺ is able to substitute positions of Ti⁴⁺ in SrTiO₃ [28]. From our results, in combination with Fig. 1, we can conclude that the catalyst doped with Mn showed the incorporation of Mn⁴⁺ in Ti⁴⁺ sites, while in the case of the Cu-doped catalyst, some Cu was segregated to the surface in CuO form, so only some Cu was incorporated into the perovskite. Table 2 shows the quantitative analyses calculated by XPS. This table shows an appropriate relation among elements corresponding with SrTiO₃. In addition, high content of metal-dopant is observed on the surface, which can be favorable for the catalytic properties.

Fig. 5 shows the analysis of the oxygen 1 s for each catalyst. This figure reveals the existence of three different species of oxygen on the surface of all catalysts. The most intensive signal in these catalysts appears at 529.1 eV which correspond to lattice oxygen in SrTiO₃ [26,46]. The second peak in intensity is deconvoluted at 531.0 eV. This oxygen correspond to the bonding C=O in carbonates [46] and have a good agreement with the presence of SrCO₃

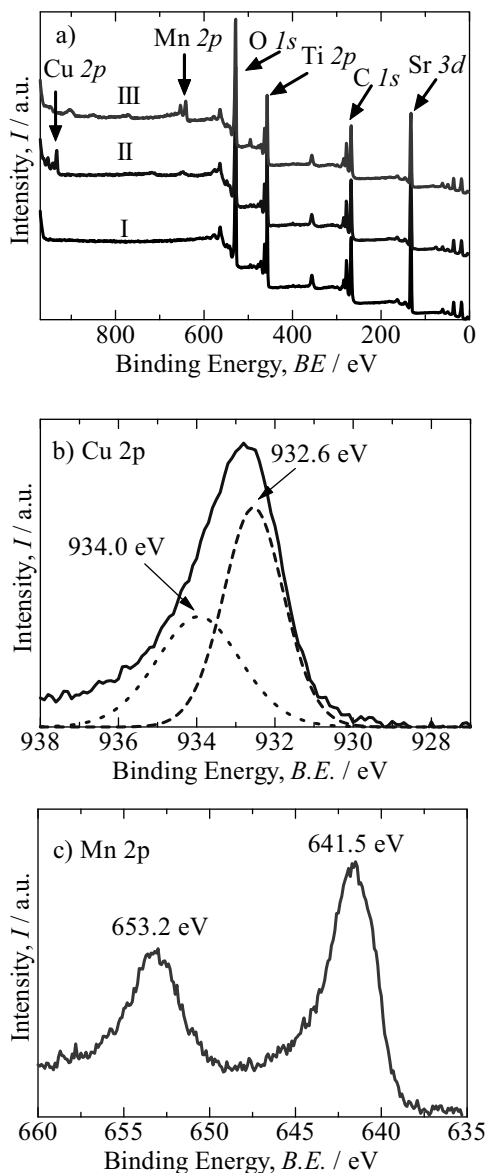


Fig. 4. XPS spectra of samples synthesized in this work: a) General spectra where (I) SrTiO_3 , (II) $\text{SrTi}_{1-x}\text{Cu}_x\text{O}_3$ and (III) $\text{SrTi}_{1-x}\text{Mn}_x\text{O}_3$, b) Cu 2p region spectrum of $\text{SrTi}_{1-x}\text{Cu}_x\text{O}_3$ and c) Mn 2p region spectrum of $\text{SrTi}_{1-x}\text{Mn}_x\text{O}_3$.

showed in the XRD results. Finally, the peak at 532.4 eV is related with the weakly bonded oxygen chemisorbed [26]. **Fig. 5c**, which corresponds to the catalyst doped with Mn, showed the highest peak area for this last oxygen specie as it is also demonstrated with the $[\text{O}_{\text{ads}}\text{ (532.4 eV)}/\text{O}_{\text{lat}}\text{ (529.1 eV)}]$ ratio in **Table 1**. This result confirms that the highest amount of adsorbed oxygen species take place on the catalyst doped with Mn, which can result in better catalytic activity as it will be discussed in the next section.

TPR analyses were also carried out for all the catalysts (see **Fig. 6**) and differences can be seen as a function of the dopant used. The SrTiO_3 base perovskite showed one high and well defined reduction peak at high temperature (780°C), which is related with the reduction of Ti^{4+} species [47]. This peak appears in all catalysts, being the temperature of the maximum of the peak slightly higher for the raw perovskite (780°C) compared with that one obtained for the other two perovskites (766°C). In addition, the hydrogen consumption at this temperature is higher in the case of the Mn-doped perovskite compared with the other two (**Table 1**), which indicates a higher reducibility of these species when Mn is added to the structure of

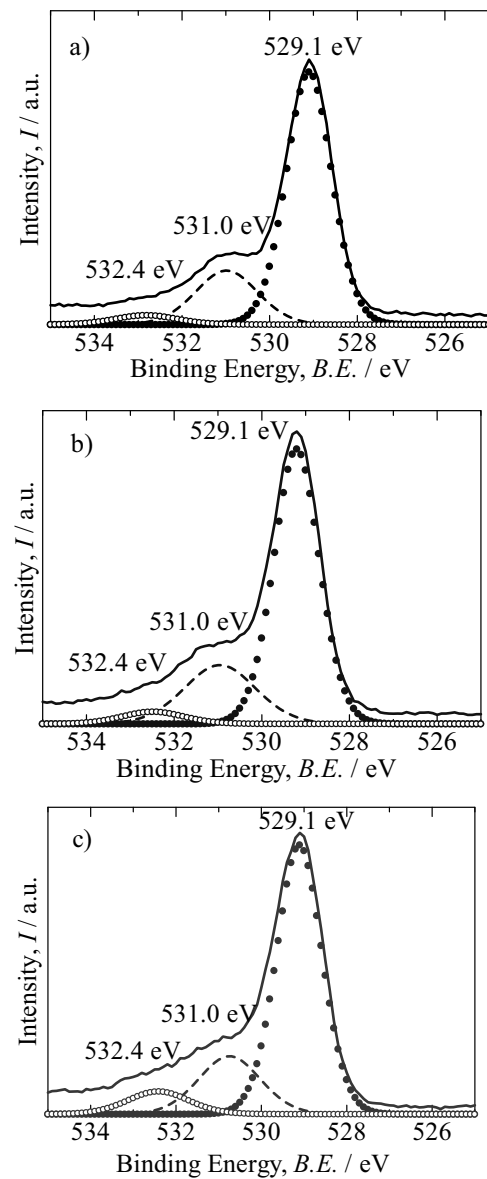


Fig. 5. XPS spectra of O 1s region of samples synthesized in this work: a) SrTiO_3 , b) $\text{SrTi}_{1-x}\text{Cu}_x\text{O}_3$ and c) $\text{SrTi}_{1-x}\text{Mn}_x\text{O}_3$.

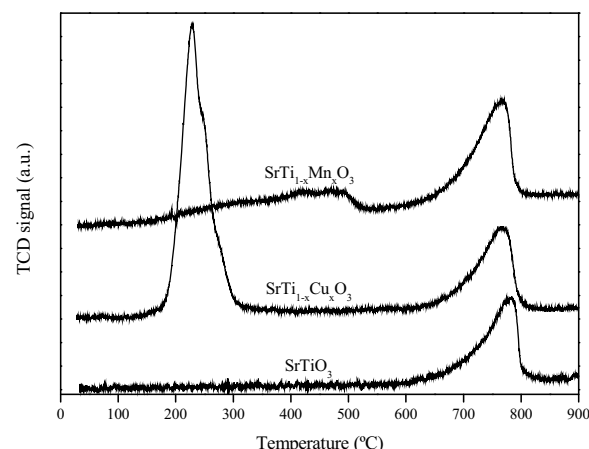


Fig. 6. Temperature-programmed reduction profiles of samples synthesized in this work and calcined at 600°C .

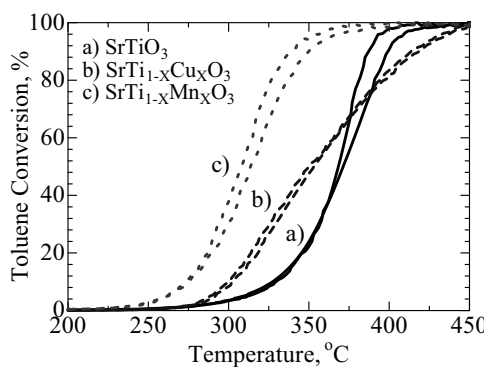


Fig. 7. Light-off curves of toluene catalytic oxidation as a function of temperatures during the third catalytic assay.

Table 3

Temperatures at 50% and 90% of light-off toluene catalytic conversion for three consecutive runs using the samples synthesized in this work as catalyst.

	SrTiO ₃ (°C)	SrTi _{1-x} Cu _x O ₃ (°C)	SrTi _{1-x} Mn _x O ₃ (°C)
1st run	50%	336	343
	90%	354	398
2nd run	50%	355	348
	90%	371	407
3rd run	50%	370	348
	90%	385	412

the perovskite. Perovskite doped with Cu also shows a high and well defined reduction peak at 230 °C, probably due to the reduction of the CuO particles towards Cu⁰. The presence of CuO particles in the Cu-doped perovskite was also observed by XRD. However, in the case of the Mn-doped perovskite a much smaller and broad reduction peak was observed in the range 160–530 °C, probably due to the reduction of Mn⁴⁺ species towards Mn²⁺ species. The long range and low intensity of this reduction peak is probably due to the high dispersion of Mn and the presence of species with different interaction with the perovskite structure. Using the H₂-consumption values obtained from these two peaks obtained for doped catalysts it is possible to calculate the reduction degree of Cu and Mn in the doped perovskites (Table 1) taking into account the actual amount of these metals determined by ICP (4.48%wt. and 1.96%wt., respectively). The reduction degree was much higher in the case of the Cu-doped perovskite, showing its lower interaction with the perovskite structure. The difference in the reduction profiles observed for the Cu- and Mn-doped perovskites is in good agreement with the characterization results of the catalysts showed above, indicating that Mn was effectively introduced in the perovskite structure while Cu was mostly not introduced and remain as CuO particles on the surface.

3.2. Toluene catalytic oxidation tests

Fig. 7 shows the catalytic test of each catalyst after the third assay of the light-off toluene oxidation. In doped catalysts, either Cu or Mn, no appreciable deactivation was detected during the three runs, as it can be observed in Fig. 8a and b for the Mn- and Cu-doped catalysts, respectively. In contrast, raw SrTiO₃ showed a clearly deactivation after each run as it can be observed in Fig. 8c. According with these results, the addition of metals-doping as Cu and Mn enhances the stability of the catalysts during the catalytic process. In addition, Table 3 shows the temperatures corresponding to 50% and 90% of toluene conversion during each catalytic run, which are comparable with previous catalytic results reported in literature for perovskites materials [36,48–52]. Results observed confirm the stability of doped-catalysts because the difference among each cycle

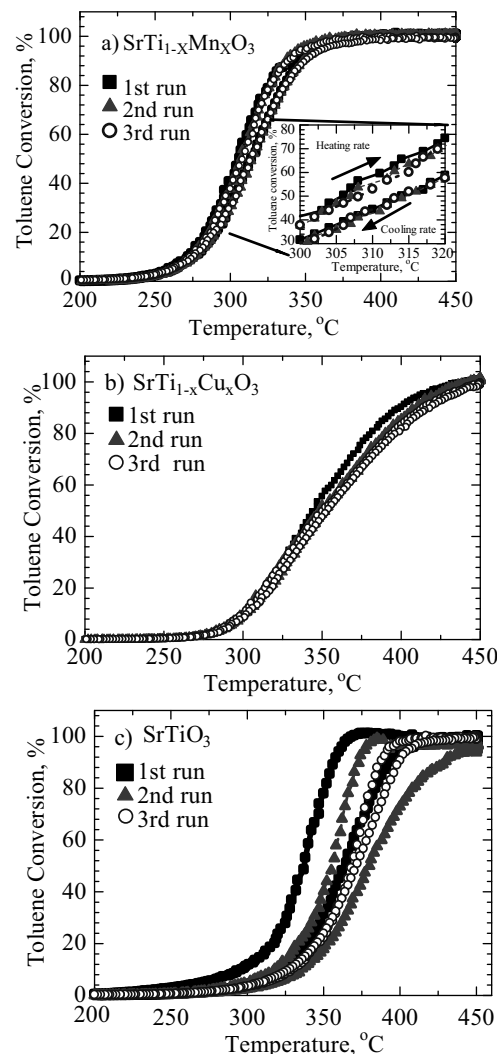


Fig. 8. Light-off curves of the toluene catalytic oxidation during three consecutive runs using catalysts synthesized in this work. a) SrTi_{1-x}Mn_xO₃, b) SrTi_{1-x}Cu_xO₃ and c) SrTiO₃.

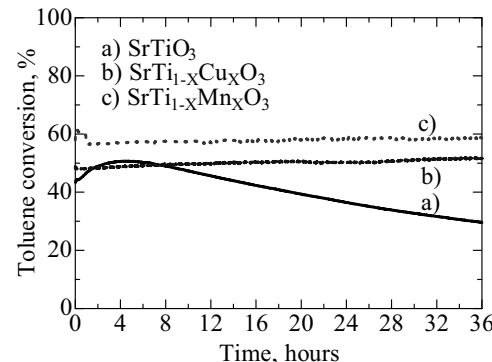


Fig. 9. Light-off experiments of toluene catalytic oxidation as a function of time at T_{50%}.

is inside the experimental error ($\pm 5^\circ\text{C}$), while the undoped catalyst showed a difference up to 19 °C. This behavior is confirmed during the long term stabilization test at 50% of toluene conversion (Fig. 9). This experiment was carried out at 336 °C, 343 °C and 315 °C for SrTiO₃, SrTi_{1-x}Cu_xO₃ y SrTi_{1-x}Mn_xO₃, respectively, which correspond to the T_{50%} obtained for each catalyst as it is

shown in **Table 3**. However, temperature at 315 °C for $\text{SrTi}_{1-x}\text{Mn}_x\text{O}_3$ was chosen because represents the temperature at 50% of toluene conversion during the cooling rate in **Fig. 8a**. It can be observed that doped-catalysts showed high stability during 36 h, whereas the raw SrTiO_3 than presented a clearly deactivation. It is worthy to mention that the excellent stability of the Mn-doped catalyst at 58% of toluene conversion correspond to the toluene decomposition percentage during the heating rate observed in **Fig. 8a**. Moreover, the catalyst doped by Mn showed a littler displacement in $T_{50\%}$ between the cooling rate and the heating rate, whereas the $T_{50\%}$ was the same in heating and cooling rates for other catalysts. Besides than in the catalytic stability, the addition of dopants has also a strong influence in the catalytic activity. The results showed in **Fig. 7** clearly indicate that the incorporation of Mn enhances the toluene catalytic conversion. This behavior can be attributed to the higher amount of oxygen weakly adsorbed species on the surface of this catalyst, as was observed by XPS; which is related with a higher amount of oxygen vacancies in the perovskite surface [53]. It is reported that toluene oxidation by perovskites follow a suprafacial mechanism [16,54] and more available oxygen on the surface could promote the toluene conversion. Increasing the temperature is observed that the catalytic activity of the catalyst doped by Mn remain the highest one. In contrast, the catalyst doped by Cu have lower $T_{50\%}$ values than the undoped perovskite (**Table 3**), but its catalytic activity is lower at high temperatures. As it is observed in **Table 1**, the $\text{O}_{\text{ads}}/\text{O}_{\text{lat}}$ ratio is quite similar showing the effect of Cu-doped at low temperatures. It is reported that CuO on the surface can be reduced at temperatures between 200 and 360 °C, however Cu inside the SrTiCuO_3 structure is hardly reduced [26]. This Cu reduction behavior can explain the activation of the catalyst doped with Cu at lower temperature than the undoped one. At higher temperatures oxygen migration from the lattice to the surface can occur in the undoped sample by ion mobility mechanism [55]. The driving force of this mechanism can be the bulk-surface gradient of oxygen in the catalyst. This oxygen mobility can explain the abrupt jump of the conversion of toluene in the undoped catalyst resulting in lower $T_{90\%}$ values than the catalyst doped by Cu shown in **Table 3**.

4. Conclusions

SrTiO_3 doped with Cu and Mn was successfully synthesized by one pot hydrothermal method. This method has proven to be effective to synthesize perovskite with dendritic morphology and, as a consequence, with high specific surface area ($22\text{--}28 \text{ m}^2 \text{ g}^{-1}$), which makes these materials promising catalysts for the future application in catalytic combustion reactions. The Mn-doped was incorporated into the B-site of SrTiO_3 structure, according to XPS analyses, whereas the Cu was mostly not introduced and remain as CuO particles on the perovskite surface. The Mn and Cu-doped perovskites ($\text{SrTi}_{1-x}\text{B}_x\text{O}_3$) provide higher catalytic stability, during 36 h time on stream with no apparent deactivation, compare to the un-doped perovskite one, which was deactivated after 8 h of toluene oxidation reaction. This fact confirm that the metal-dopant incorporation into the perovskite structure and the relative cations segregation on the perovskite surface avoid the oxidation deactivation. The catalytic activity trend in terms of $T_{90\%}$, from the lowest to the highest, followed the order: Mn-doped < undoped < Cu-doped, where the Mn-doped perovskite catalyst exhibited the best catalytic performance in the toluene oxidation, related to the higher amount of adsorbed oxygen species on its surface and higher reducibility at low temperature. This study presents an attractive and economic method to prepare doped-perovskite oxide catalysts with original morphology, which allows to understand the effect of

the co-cation added on the physico-chemical and redox properties as well as to control the stability in oxidation reactions.

Acknowledgements

SSV and ACL want to express their gratitude to the administration of Civil Engineering Faculty and Materials Construction Laboratory from UANL for the facilities provided during the realization of this work. Also SSV wants to thanks to thematic network of nanoscience and nanotechnology from CONACYT for the partial economic support during the synthesis of the catalysts.

References

- [1] Indoor Air Quality: Organic Pollutants, Report on a WHO Meeting, EURO Report and Studies, 1989, 1–70.
- [2] USEPA, Reducing Risk: Setting Priorities and Strategies for Environmental Protection, U.S. Environmental Protection Agency, 1990.
- [3] Thematic Strategy on Air Pollution, Communication from the Commission to the Council and the European Parliament, Commission of the European Communities, COM (2005) 446 final, Brussels, 2005.
- [4] Contents of New Emissions Regulation of Volatile Organic Compounds, Press Release 2005, Ministry of Environment, Government of Japan.
- [5] The clean air act amendments 1990. A Guide for small businesses, US, EPA, September 1992.
- [6] K. Acuna-Askar, M.A. de la Torre Torres, M.J. Guerrero-Munoz, M.T. Garza-Gonzalez, B. Chavez-Gomez, I.P. Rodriguez-Sanchez, H.A. Barrera-Saldana, *Water Sci. Technol.* 53 (11) (2006) 197–204.
- [7] Y. Su, X. Zhang, X. Wei, J. Kong, F. Xia, W. Lei, R. He, *J. Hazard. Mater.* 274 (2014) 367–375.
- [8] N. Asenjo, P. Álvarez, M. Granda, C. Blanco, R. Santamaría, R. Menéndez, *J. Hazard. Mater.* 192 (2011) 1525–1532.
- [9] C. Ma, R. Ruan, *Appl. Clay Sci.* 80–81 (2013) 196–201.
- [10] B. Liu, X. Li, Q. Zhao, J. Ke, J. Liu, S. Liu, M. Tadé, *J. Colloid Interface Sci.* 438 (2015) 1–6.
- [11] D. Vildozo, R. Portela, C. Ferronato, J.M. Chovelon, *Appl. Catal. B* 107 (2011) 347–354.
- [12] M. Tasbihi, U.L. Stangar, U. Cernigoj, J. Jirkovsky, S. Bakardjieva, N.N. Tusar, *Catal. Today* 161 (2011) 181–188.
- [13] E. Rezaei, J. Soltan, N. Chen, J. Lin, *Chem. Eng. J.* 214 (2013) 219–228.
- [14] S. Jiang, E.S. Handberg, F. Liu, Y. Liao, H. Wang, *Appl. Catal. B* 160–161 (2014) 716–721.
- [15] Z. Liu, J. Chen, Y. Peng, *J. Hazard. Mater.* 256–257 (2013) 49–55.
- [16] C. Zhang, Y. Guo, Y. Guo, G. Lu, A. Boreave, L. Retailleau, A. Baylet, A. Giroir-Fendler, *Appl. Catal. B* 148–149 (2014) 490–498.
- [17] K. Ji, H. Dai, J. Deng, H. Jiang, L. Zhang, H. Zhang, Y. Cao, *Chem. Eng. J.* 214 (2013) 262–271.
- [18] J. Zhu, H. Li, L. Zhong, P. Xiao, X. Xu, X. Yang, Z. Zhao, J. Li, *ACS Catal.* 4 (2014) 2917–2940.
- [19] C. Zhang, C. Wang, W. Zhan, Y. Guo, Y. Guo, G. Lu, A. Baylet, A. Giroir Fendler, *Appl. Catal. B* 129 (2013) 509–516.
- [20] C. Zhang, C. Wang, W. Zhan, Y. Guo, Y. Guo, G. Lu, A. Baylet, A. Giroir Fendler, *Appl. Catal. B* 134–135 (2013) 310–315.
- [21] A. Rothschild, W. Meneskou, H.L. Tuller, E. Ivers-Tiffée, *Chem. Mater.* 18 (2006) 3651–3659.
- [22] N. Li, A. Boreave, J.P. Deloume, F. Gaillard, *Solid State Ionics* 179 (2008) 1396–1400.
- [23] Y. Sekine, D. Mukai, Y. Murai, S. Tochiya, Y. Izutsu, K. Sekiguchi, N. Hosomura, H. Arai, E. Kikuchi, Y. Sugiura, *Appl. Catal. A* 451 (2013) 160–167.
- [24] J. Wang, S. Yin, M. Komatsu, Q. Zhang, F. Saito, T. Sato, J. Phochem. *Photobiol. A* 165 (2004) 149–156.
- [25] T. Ohno, T. Tsubota, Y. Nakamura, K. Sayama, *Appl. Catal. A* 288 (2005) 74–79.
- [26] F.E. López-Suárez, S. Parres-Escalpés, A. Bueno-López, M.J. Illán-Gómez, B. Ura, J. Trawczynski, *Appl. Catal. B* 93 (2009) 82–89.
- [27] F.E. López-Suárez, M.J. Illán-Gómez, A. Bueno-López, J. Anderson, *Appl. Catal. B* 104 (2011) 261–267.
- [28] G. Wu, P. Li, D. Xu, B. Luo, Y. Hong, W. Shi, C. Liu, *Appl. Surf. Sci.* 333 (2015) 39–47.
- [29] B. Ura, J. Trawczynski, A. Kotarba, W. Bieniasz, M.J. Illán-Gómez, A. Bueno-López, F.E. López-Suárez, *Appl. Catal. B* 101 (2011) 169–175.
- [30] R. Niishiro, S. Tanaka, A. Kudo, *Appl. Catal. B* 150–151 (2014) 187–196.
- [31] S.T. Huang, W.W. Lee, J.L. Chang, W.S. Huang, S.Y. Chou, C.C. Chen, *J. Taiwan Inst. Chem. Eng.* 45 (2014) 1927–1936.
- [32] K. Takehira, T. Shishido, M. Kondo, *J. Catal.* 207 (2002) 307–316.
- [33] K. Urasaki, K. Tokunaga, Y. Sekine, M. Matsukata, E. Kikuchi, *Catal. Commun.* 9 (2008) 600–604.
- [34] B. Bialobok, J. Trawczynski, T. Rzadki, W. Mista, M. Zawadzki, *Catal. Today* 119 (2007) 278–285.
- [35] J.S. Yoon, Y.H. Kim, E.J. Lee, M.J. Ji, B.H. Choi, H.J. Hwang, *Electron. Mater. Lett.* 7 (2011) 209–213.
- [36] S. Rousseau, S. Loridan, P. Delichere, A. Boreave, J.P. Deloume, P. Vernouxet, *Appl. Catal. B: Environ.* 88 (2009) 438–447.

[37] S. Kaliaguine, A. Van Neste, V. Szabo, J.E. Gallot, M. Bassir, R. Muzychuk, *Appl. Catal. A: Gen.* 209 (2001) 345–358.

[38] V. Kalyani, B.S. Vasile, A. Ianculescu, A. Testino, A. Carino, M.T. Buscaglia, V. Buscaglia, P. Nanni, *Cryst. Growth Des.* 15 (2015) 5712–5725.

[39] Z. Zheng, B. Huang, X. Qin, X. Zhang, Y. Dai, *J. Colloid Interface Sci.* 358 (2011) 68–72.

[40] P. Jayabal, V. Sasirekha, J. Mayandi, K. Jeganathan, V. Ramakrishnan, *J. Alloys Compd.* 586 (2014) 456–461.

[41] H.A.J.L. Mourao, O.F. Lopes, C. Ribeiro, V.R. Mastelaro, *Mater. Sci. Semicond. Process.* 30 (2015) 651–657.

[42] K. del Ángel-Sánchez, O. Vázquez-Cuchillo, M. Salazar-Villanueva, J.F. Sanchez-Ramirez, A. Cruz-López, A. Aguilar-Elguezabal, *J. Sol-Gel Sci. Technol.* 52 (2) (2011) 360–365.

[43] M. Lencka, R. Riman, *Chem. Mater.* 5 (1993) 61–70.

[44] Y. Oaki, H. Imai, *Cryst. Growth Des.* 3 (5) (2003) 711–716.

[45] A. Giroir-Fendler, M. Alves-Fortunato, M. Richard, C. Wang, J.A. Díaz, S. Gil, C. Zhang, F. Can, N. Bion, Y. Guo, *Appl. Catal. B* 180 (2016) 29–37.

[46] W.Y. Hernández, M.N. Tsampas, C. Zhao, A. Boreave, F. Bosselet, P. Vernoux, *Catal. Today* 258 (2015) 525–534.

[47] H.R. Gurav, R. Bobade, V.L. Das, S. Chilukuri, *Ind. J. Chem.* 51A (2012) 1339–1347.

[48] G. Peccati, M.G. Jiliberto, E.J. Delgado, L.E. Cadus, J.L.G. Fierro, *J. Chem. Technol. Biotechnol.* 86 (2011) 1067–1073.

[49] S. Irusta, M.P. Pina, M. Menéndez, J. Santamaría, *J. Catal.* 179 (1998) 400–412.

[50] M. Alifanti, M. Florea, V.I. Pârvulescu, *Appl. Catal. B: Environ.* 70 (2007) 400–405.

[51] S.A. Hosseini, M.T. Sadeghi, A. Alemi, A. Niaezi, D. Salari, L. Kafi-Ahamadi, *Chin. J. Catal.* 31 (2010) 747–750.

[52] M. Florea, M. Alifanti, V.I. Parvulescu, D. Mihaila-Tarabasanu, L. Diamandescu, M. Feder, C. Negrila, L. Frunza, *Catal. Today* 141 (2009) 361–366.

[53] N.A. Merino, B.P. Barbero, P. Eloy, L.E. Cadús, *Appl. Surf. Sci.* 253 (2006) 1489–1493.

[54] R.J. Vorhoeve, J.P. Remeika, D.W. Johnson, *Science* 180 (1973) 62–64.

[55] E.V. Tsipis, M.V. Patrakeev, V.V. Kharton, A.A. Yaremchenko, G.C. Mather, A.L. Shaula, I.A. Leonidov, V.L. Kozhevnikov, J.R. Frade, *Solid State Sci.* 7 (2005) 355–365.